HEALTH AND MEDICINE

Copyright © 2025 The Authors, some rights reserved; exclusive licensee American Association for the Advancement of Science. No claim to original U.S. Government Works. Distributed under a Creative Commons Attribution NonCommercial License 4.0 (CC BY-NC).

Reducing hepatitis C diagnostic disparities with a fully automated deep learning–enabled microfluidic system for HCV antigen detection

Hui Chen[1], Yuxin Gao[1], Gaojian Li[1], Manasvi Alam[1], Srisruthi Udayakumar[1], Qazi Noorul Mateen[1], Sahar Rostamian[1], Katherine Cilley[1], Sungwan Kim[1], Giwon Cho[1], Juyong Gwak[1], Yixuan Song[1], Joseph Michael Hardie[1], Manoj Kumar Kanakasabapathy[1], Hemanth Kandula[1], Prudhvi Thirumalaraju[1], Younseong Song[1], Azim Parandakh[1], Arafeh Bigdeli[1], Gregory P. Fricker[2], Jenna Gustafson[2], Raymond T. Chung[2], Jorge Mera[3], Hadi Shafiee[1]*

Viral hepatitis remains a major global health issue, with chronic hepatitis B (HBV) and hepatitis C (HCV) causing approximately 1 million deaths annually, primarily due to liver cancer and cirrhosis. More than 1.5 million people contract HCV each year, disproportionately affecting vulnerable populations, including American Indians and Alaska Natives (AI/AN). While direct-acting antivirals (DAAs) are highly effective, timely and accurate HCV diagnosis remains a challenge, particularly in resource-limited settings. The current two-step HCV testing process is costly and time-intensive, often leading to patient loss before treatment. Point-of-care (POC) HCV antigen (Ag) testing offers a promising alternative, but no FDA-approved test meets the required sensitivity and specificity. To address this, we developed a fully automated, smartphone-based POC HCV Ag assay using platinum nanoparticles, deep learning image processing, and microfluidics. With an overall accuracy of 94.59%, this cost-effective, portable device has the potential to reduce HCV-related health disparities, particularly among AI/AN populations, improving accessibility and equity in care.

INTRODUCTION

Viral hepatitis remains one of the foremost contributors to global health challenges, ranking within the top 10 causes of morbidity and mortality worldwide. The World Health Organization (WHO) has reported that around 1 million deaths annually are attributable to chronic hepatitis B virus (HBV) and hepatitis C virus (HCV), largely due to severe complications such as liver cirrhosis and hepatocellular carcinoma. Moreover, more than 1.5 million people are newly infected with hepatitis C each year (*1*). Managing HCV infection effectively, especially in populations with substantial health disparities, poses considerable obstacles. Vulnerable groups include those in resource-constrained environments, rural areas, economically disadvantaged regions, migrants, and displaced individuals. For instance, American Indians and Alaska Natives (AIs/ANs) have a reported incidence of new HCV infections at 2.9 cases per 100,000 compared to 0.5 cases per 100,000 among African Americans and 1.2 cases per 100,000 in non-Hispanic whites, with markedly higher mortality rates compared to other ethnic and racial groups (*2*, *3*). Historical and generational trauma including loss of population, land, and culture has contributed to the health inequities seen among AI/AN people today (*4*).

In response to the high prevalence of HCV among AI/AN populations and the introduction of effective direct-acting antivirals (DAAs), the Cherokee National Health Services (CNHS) implemented enhanced HCV testing strategies in October 2012, in alignment with the 2012 US Centers for Disease Control and Prevention (CDC) guidelines and the recommendations of the US Preventive Services Task Force. These initiatives included the integration of reminders in the electronic health record system to support clinical decision-making (*2*). The implementation of these testing protocols at CNHS resulted in substantial reductions in patient wait times, travel requirements, and the number of necessary clinical visits when compared to traditional screening methods. Notably, the proportion of AI/AN individuals in Oklahoma undergoing initial HCV testing increased fivefold between 2012 and 2015 following the adoption of these policies (*2*). However, despite these advancements, the demand for confirmatory HCV RNA testing has surged, and a substantial portion of individuals identified as HCV antibody positive did not receive confirmatory HCV RNA testing (*2*).

Even with the advent of DAA therapies, which are characterized by their ease of use (once-daily oral dosing) and high efficacy (achieving cure rates greater than 95%) (*5*, *6*), the early and accurate diagnosis of active HCV infection continues to be a substantial challenge, particularly in resource-limited settings and among populations disproportionately affected by HCV, such as AIs/ANs (*7*). Globally, it is estimated that only 21% of individuals infected with HCV are actually diagnosed (*1*, *8*–*10*). To meet the WHO's HCV elimination targets established in 2016, which aim for an 80% reduction in the incidence of new HCV infections and a 65% reduction in HCV-related mortality by 2030, there must be a substantial increase in HCV screening efforts to identify 90% and treat at least 80% of the estimated 58 million individuals living with HCV worldwide (*11*, *12*).

One of the major barriers to connecting individuals infected with HCV to effective DAA treatment is the reliance on a two-step HCV testing process (*13*, *14*). This process involves initial HCV antibody screening followed by confirmatory HCV RNA testing, which is costly, time-consuming, inconvenient, and often leads to suboptimal

[1]Division of Engineering in Medicine, Division of Renal Medicine, Department of Medicine, Brigham and Women's Hospital, Harvard Medical School, Boston, MA 02139, USA. [2]Liver Center, Gastrointestinal Division, Massachusetts General Hospital, Harvard Medical School, Boston, MA 02114, USA. [3]Infectious Diseases, Cherokee Nation Health Services, Tahlequah, OK, 74464, USA.
*Corresponding author. Email: hshafiee@bwh.harvard.edu

outcomes. As a result, many individuals diagnosed with HCV antibodies disengage from care before receiving confirmatory HCV RNA testing and appropriate treatment (*8*, *15*, *16*). HCV antibody testing, which cannot distinguish between resolved (R-HCV) and viremic (V-HCV) HCV infection, is unable to detect acute HCV infection and is not suitable for individuals who are immunocompromised, on immunosuppressive therapy, or undergoing hemodialysis (*17*, *18*). Consequently, when HCV antibody tests return positive results, additional HCV RNA testing is necessary to confirm active infection.

Currently available HCV RNA assays, including point-of-care (POC) HCV RNA tests, are predominantly laboratory-based, expensive, and often inaccessible to populations that are disproportionately affected by HCV, including AIs/ANs (*13*, *15*, *19*). The development of low-cost, rapid, sensitive, and specific POC HCV antigen (Ag) tests offers a promising alternative for one-step HCV screening and diagnosis, particularly for populations that are disproportionately affected by HCV and those in resource-limited settings (*20*–*29*). In these environments, the use of POC HCV Ag diagnostics instead of HCV RNA testing is not only cost-effective but also operationally advantageous, facilitating a streamlined, one-step process for HCV diagnosis and linkage to care (*30*). HCV Ags—which are detectable in whole blood, plasma, or serum regardless of the presence of HCV antibodies—serve as reliable surrogate markers for active HCV infection and viral replication (*23*–*29*). Notably, HCV Ags, similar to HCV RNA, are detectable in the bloodstream during the acute phase of infection, well before antibodies are produced (*31*).

Now, there are no commercially available and US Food and Drug Administration (FDA)–approved POC HCV Ag testing devices. The existing HCV Ag assays have been primarily developed for laboratory use, making them relatively expensive and, more importantly, lacking the necessary sensitivity and specificity, particularly when testing samples with clinically notable low viral loads (<1000 IU/ml). This limitation has restricted their clinical utility (*32*–*40*). The reported limits of detection (LOD) for the developed HCV Ag diagnostics range from 3000 to 10,000 IU/ml, in contrast to the LOD of 12 to 15 IU/ml achieved by polymerase chain reaction (PCR)–based assays (*40*–*42*).

Although the 2016 European Association for the Study of the Liver (EASL) guidelines and the WHO Global Hepatitis Report have recognized HCV Ag testing as a feasible alternative to HCV RNA testing, particularly in resource-limited settings, and have conditionally endorsed the ARCHITECT HCV Ag assay as an in vitro diagnostic tool for acute HCV infection, the WHO acknowledges its limitations in accurately identifying individuals with clinically relevant low viral loads (<1000 IU/ml) (*20*, *43*). For example, the Abbott Architect HCV cAg assay demonstrated a sensitivity range of 64.7 to 81.9% when tested with HCV serum samples featuring viral loads of $<10^4$ IU/ml and 0.0 to 19.7% when tested with samples with viral loads of <1000 IU/ml (*38*, *39*). In a recent clinical study involving 744 cases, the sensitivity of the HCV Ag test was reported as 82.1% (*20*).

Currently available serological assays for HCV detection do not meet the requirements for accurate, sensitive, specific, low-cost, user-friendly, and POC detection of HCV Ag using small volumes of whole blood samples, such as those obtained from fingerpricks (*44*). For instance, a lateral flow assay developed by Wang *et al.* (*45*) for HCV core Ag (cAg) detection exhibited a sensitivity of 10.71% compared to RNA-based assays when samples with viral loads between 10^3 and 10^4 copies/ml were used (*45*). This underscores the urgent need for the development of cost-effective, scalable diagnostics that allow for on-site, one-step, rapid HCV Ag testing, particularly for high-risk and disproportionately affected populations, including AI/ANs (*46*). The deployment of these rapid POC HCV tests has the potential to substantially improve HCV infection management by enabling immediate treatment decisions and reducing patient loss to follow-up (*10*, *47*). The critical need for the development of POC HCV Ag diagnostics was extensively discussed by national HCV experts during a webinar titled "Identifying high-priority diagnostic approaches for Advancing hepatitis C elimination in the US," organized by the Association of Public Health Laboratories (APHL) in collaboration with the CDC's Division of Viral Hepatitis in October 2021 (*48*).

Here, we report the development and validation of a microfluidic-based POC HCV cAg assay using an all-in-one handheld automated microfluidic system (AAS). This assay was designed to be user-friendly, cost-effective, and portable, with the aim of improving accessibility for underserved community members, particularly within the AI/AN populations, ultimately reducing disparity in HCV-related care. This assay achieves successful HCV detection with a sample-to-answer time of approximately 23 min using a fingerprick volume (50 μl) of patient plasma sample. It can reliably detect HCV RNA concentrations as low as 574 IU/ml. Compared to reverse transcription PCR (RT-PCR) methods, the HCV cAg POC test demonstrated an accuracy exceeding 94.59% [95% confidence interval (CI), 86.73 to 98.51%] with a positive percent agreement of 98.04% (95% CI, 88.06 to 99.71%) and a negative percent agreement of 86.96% (95% CI, 68.87 to 95.26%) in a clinical validation study with 74 clinical patient plasma samples including 36 samples collected from AI/ANs.

RESULTS

Characterizations of the AAS

We developed the AAS that enables automated sample processing on the disposable cartridge preloaded with assay reagents through sequential and oscillatory sample and reagent flows for the rapid and sensitive detection of HCV cAg as illustrated in Fig. 1 and fig. S1. The disposable microfluidic cartridge is composed of one waste chamber to self-contain all the reagents after running the test, one intestine-shaped test channel, one intestine-shaped control channel, and 14 reservoirs for on-chip storage of assay reagents and buffering liquid during the oscillatory flows, as shown in fig. S2. The test and control channels on the cartridge are coated with capture antibody against HCV cAg and polyclonal goat anti-mouse immunoglobuin G (IgG) (Fc specific) antibody to capture mouse antibody coated Pt nanoprobes, respectively. Pt nanoprobe-labeled HCV cAg complexes are captured on the surface of the test channel to confirm the presence of HCV cAg, while free Pt nanoprobes are captured on the surface of the control channel to indicate successful sample flow and nanoprobe activity. To prevent interference or cross-talk between the assay reagents in the on-chip reservoirs during storage and shipment, retention burst valves have been incorporated into the system, as illustrated in fig. S3 and movie S1.

The assay is initiated by pressing the start switch on the reader, activating a code that controls a mini pump and a solenoid valve to direct different assay reagents to flow sequentially and oscillate through the test/control channels. This periodic oscillatory flow substantially enhances mixing and binding performance between the target molecules in the sample solution and the surfaces functionalized

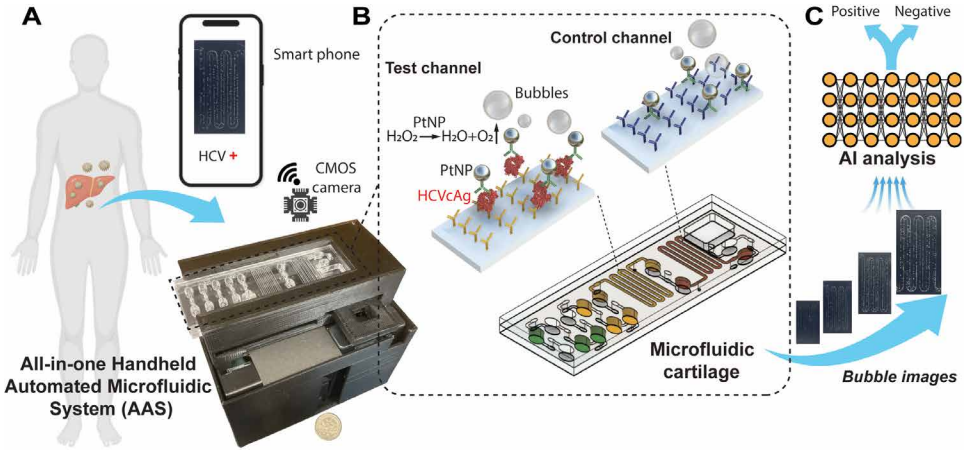

Fig. 1. AAS for POC HCV detection. (**A**) Overview of the AAS for HCV detection. A patient serum sample is loaded on a microfluidic cartridge with preloaded assay reagents and is automatically processed using a standalone optical reader. The optical image data are captured by a standalone wireless camera and transmitted to a smartphone for analysis using a deep learning–enabled smartphone application. (**B**) Working principle of the bubbling assay in the microfluidic cartridge. The test channel and control channel of the cartridge are coated with capture antibody against the HCV core antigen (HCV cAg) and polyclonal goat anti-mouse IgG (Fc-specific) antibody (to capture the mouse antibody-coated Pt nanoprobes), respectively. Pt nanoprobe–HCV cAg complexes are captured on the surface of the test channel to confirm the presence of HCV cAg, while free Pt nanoprobes are captured on the surface of the control channel to indicate successful sample flow and nanoprobe activity. Captured Pt nanoprobes in the test and control channels catalyze the decomposition of H_2O_2 into O_2 bubbles, which can be imaged by a built-in CMOS camera to indicate the existence of HCV cAg (test channel) and the functionality of the cartridge (control channel). (**C**) Captured images are analyzed on a smartphone application using a deep learning adversarial model.

with binding ligands by expanding the effective path traveled by the fluids within the system (*49*). It also creates repeated turbulent transport within the interconnected large-scale reservoirs and increases the frequency of molecular collisions facilitated by the periodic oscillatory flows. To increase the portability and accessibility of the sensing device, we designed a simple and handheld peripheral microfluidic control system for programmable sequential flows and oscillatory flows to automatically detect HCV cAg, as shown in fig. S4. A standalone wireless imaging module was used to capture images from the AAS and wirelessly transmit the data to the smartphone application for analysis, as shown in fig. S5.

After the programmed flows pass through the two channels, Pt nanoprobe-HCV cAg complexes are captured on the surface of the test channel, and Pt nanoprobes are captured on the surface of the control channel. Pt nanoparticles catalyze the decomposition of H_2O_2 into O_2 bubbles, which can be imaged using a built-in complementary metal-oxide semiconductor (CMOS) camera for data analysis.

The mini peristaltic pump was connected to one end of the microfluidic circuit to control fluid movements by adjusting the pressures. The other end of the microfluidic circuit is always open to the atmosphere. The solenoid valve is used to regulate the connection between the first reagent reservoir and the atmosphere. There were two states of the microfluidic circuit: (i) oscillatory flow state and (ii) sequential flow state, with the transition between these states controlled by a solenoid valve, as depicted in Fig. 2 (B and C). When oscillatory flows are required to enhance mass transfer in the test/control channels, as shown in Fig. 2B, the solenoid valve is activated to connect the reaction reservoir to the atmosphere. This creates a closed circuit (red) that includes only the test/control channels and the first reagent reservoir while excluding the other reagent reservoirs from the microfluidic circuit (gray). In this mode, only the reagent in the reaction reservoir is subjected to periodic pressure changes, resulting in oscillatory flow. When sequential flow is required, as shown in Fig. 2C, the solenoid valve is turned off, disconnecting the reaction reservoir from the atmosphere and thereby including all the reagent reservoirs in the closed microfluidic circuit (red). In this mode, reagents from the series of reservoirs can sequentially enter the first reagent reservoir.

To precisely control the sequential and oscillatory flows of various assay reagents in the microfluidic channels at predetermined time intervals, we have programmed a mini peristaltic pump and a solenoid valve using a microprocessor loaded with optimized code. As shown in figs. S6 and S7, one single microprocessor was used in the circuit for synergizing the activity of a solenoid valve and a mini pump. The microprocessor is activated by simply turning on the portable power, allowing it to execute the preloaded program. To evaluate the performance of the microfluidic system in executing programmed sequential and oscillatory flows for the automatic immunoassay to detect HCV, we used colored liquids to monitor the flow steps. As demonstrated in Fig. 2D, fig. S8, and movie S2, the flow events were successfully executed automatically by the AAS, effectively meeting the requirements of the corresponding immunoassay steps. These results strongly support the accuracy of the AAS in performing programmed sequential and oscillatory flows, and they underscore its simpler peripheral microfluidic control system, which is more suitable for POC settings compared to traditional control systems. The microfluidic cartridge was designed for single use, whereas the detection module can be reused for multiple tests. The material costs for manufacturing the microfluidic cartridge and detection reader were $1.5 and $95, respectively (table S1).

The polymethyl methacrylate (PMMA) microfluidic channels were functionalized with antibodies through a layer-by-layer process (*50*, *51*). Briefly, the microchannels were first coated with poly(ethyleneimine) (PEI), followed by a coating with glutaraldehyde (GA) solution, and lastly with antibodies. The test channel was functionalized with a capture antibody against HCV cAg, while the control channel was functionalized with polyclonal goat anti-mouse

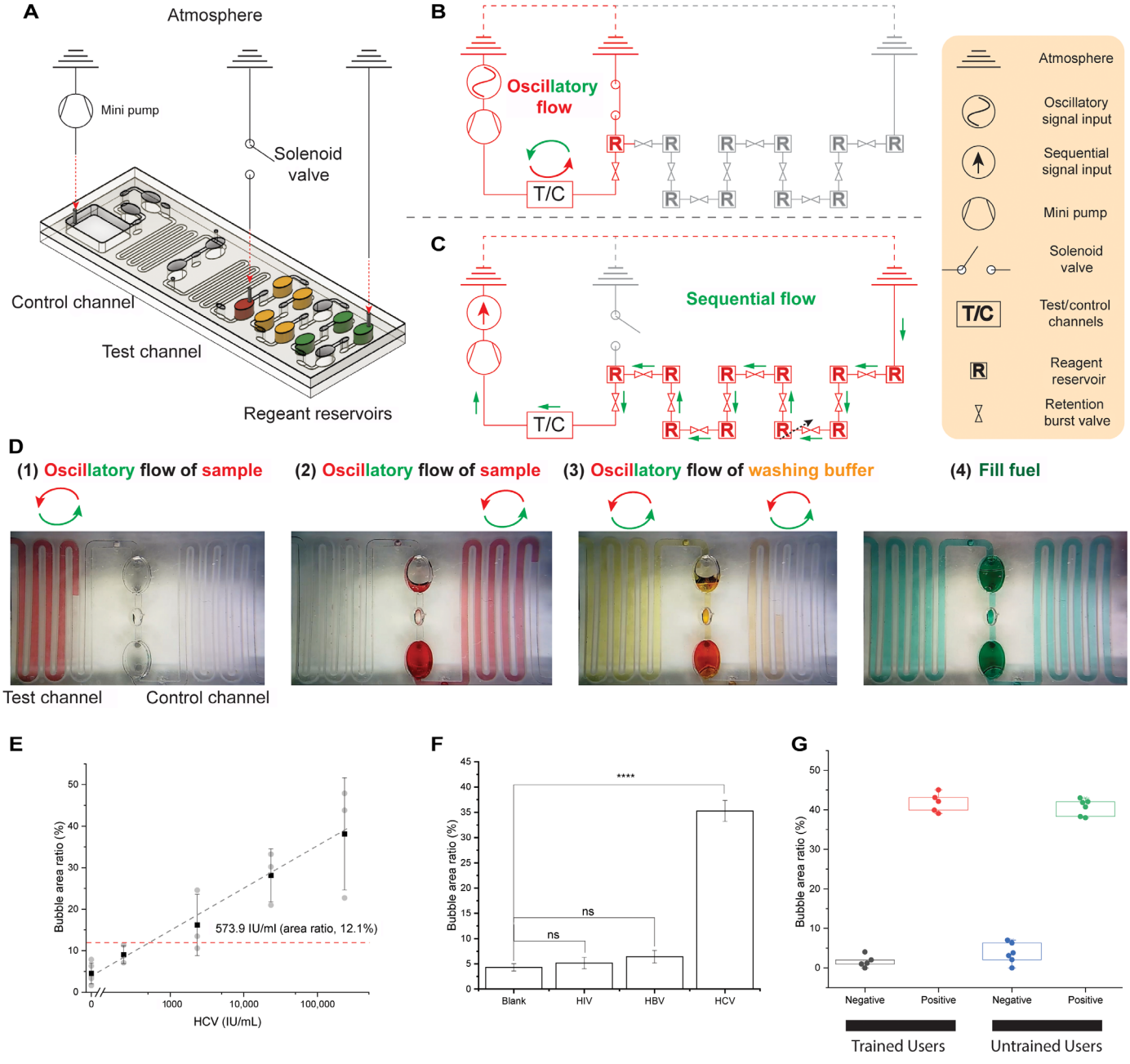

Fig. 2. AAS with simple peripheral microfluidic control system with functions of programmable sequential oscillatory flows. (**A**) Overview of the system, consisting of a mini peristaltic pump and a solenoid valve. The pump controls fluid movement, while the solenoid valve regulates the connection between the first reagent reservoir and the atmosphere. (**B** and **C**) Flow control mechanisms. In oscillatory flow mode (B), the solenoid valve opens, creating a closed circuit that includes only the test/control channels and the first reagent reservoir, allowing periodic pressure changes. In sequential flow mode (C), the valve closes, connecting all reagent reservoirs for sequential reagent delivery. (**D**) Automated immunoassay for HCV detection. Nanoprobe-labeled immunocomplexes are captured in the test channel via oscillatory flows. Excess nanoprobes enter the control channel during sequential flow. Three washes sequentially remove nonspecific nanoprobes, followed by hydrogen peroxide introduction to drive the bubbling reaction, generating a detectable signal. (**E**) Dose-response curve of AAS. Assays were performed using five HCV-negative serum samples spiked with HCV concentrations ranging from 0 to 200,000 IU/ml. The limit of detection (LOD) was determined to be 573.9 IU/ml. (**F**) Specificity test. AAS signals were compared across blank, HIV (5.3×10^5 copies/ml), HBV (4.4×10^5 IU/ml), and HCV (2.3×10^5 IU/ml) samples, confirming high specificity [$N = 3$, $P > 0.05$, not significant (ns); $^{****}P \leq 0.0001$]. (**G**) Usability test. A total of 13 users (five trained, eight untrained) tested the system, demonstrating its user-friendliness. Data points, median values, quartiles, and interquartile range whiskers are shown.

antibody (to capture the mouse antibody-coated Pt nanoprobes). To prevent nonspecific bindings, a blocking solution containing bovine serum albumin (BSA), tris buffer, and polyacrylic acid (PAA) was used to block the surface of the microfluidic channels.

Fourier transform infrared (FTIR) spectroscopy was used to confirm the successful coatings of PMMA. FTIR spectra from pristine PMMA, PEI-coated PMMA, and protein-PEI–coated PMMA were compared. The PEI-coated PMMA exhibited characteristic primary amine absorptions at 3282, 2838, and 1590 cm^{-1}, typical of N═H stretching and bending, indicating the successful coating of PEI. The protein-PEI–coated PMMA showed characteristic absorptions at 1637 cm^{-1} (C═C stretching), 1524 cm^{-1} (N─O stretching), and 1389 cm^{-1} (S═O stretching), confirming the successful antibody coating (fig. S9).

For the nanoprobe preparation, platinum nanoparticles (PtNPs) were coated with a detection antibody against HCV cAg via a straightforward process and evaluated by FTIR spectroscopy. Surface FTIR spectra of the PtNPs were compared before and after antibody functionalization. The antibody-conjugated PtNPs exhibited characteristic protein absorptions at 1652 cm^{-1} (N─H bending), 1547 cm^{-1} (N─O stretching), and 1397 cm^{-1} (C─O stretching), indicating successful antibody conjugation on the PtNPs (fig. S10).

After preparing and optimizing the assay materials, we assessed the efficacy of the AAS in capturing a target protein and generating bubble signals with the recombinant HCVcAg. A strong bubbling signal was observed within 10 min of programmed oscillatory flows, whereas a notably weaker signal was detected during static incubation (fig. S11 and movie 3). These findings validate that the programmed oscillatory flows can efficiently capture the target molecule in a short period, making AAS suitable for POC testing.

Analytical performance of AAS for HCV detection

Serially diluted human serum samples with HCV RNA concentrations ranging from 200 to 2×10^5 IU/ml were used to evaluate the assay limit of detection (LOD). A dose-response curve was plotted, and a strong correlation was observed between the target concentration and the corresponding bubbling signal (Fig. 2E and table S2). The LOD was determined by calculating the mean of the blank plus three times the SD obtained for the blank (*52*, *53*). The theoretical LOD of the assay was estimated as 573.9 IU/ml. The specificity of the assay was also evaluated using HCV samples and nontarget samples including HBV and HIV (Fig. 2F). The bubble signals due to nontarget viral samples were comparable to the blank. However, the HCV samples with similar level of viral load of 2×10^5 IU/ml generated a notable increase of bubble signal, indicating the high specificity of the AAS.

To assess the frequency of user errors, we conducted experiments involving a diverse group of individuals. These tests used samples containing the recombinant HCV cAg as the test material. The participant pool comprised a total of 13 individuals: five with specialized training and expertise related to the developed assay and eight untrained individuals with diverse backgrounds, including non-PhD graduates and undergraduate students (Fig. 2G). The participants were provided with a user instruction sheet as their only reference to conduct the testing procedure (fig. S12). Both groups achieved consistent and reproducible results, underscoring the user-friendly nature of the assay.

Development of the deep learning classifier for HCV detection

In this work, building on our previous experience (*54*), we used adaptive adversarial learning to reduce the dependence on human-annotated data and improve generalizability. This approach was used to reconfigure a smartphone-based diagnostic system, named the Smartphone-based Pathogen Detection Resource Multiplier using Adversarial Networks (SPyDERMAN), for the detection of HCV cAg (Fig. 3A). This system harnesses a library of unlabeled, diverse, and nonspecific images captured by smartphones to train deep learning models for developing on-demand image classifiers for specific targets. Deep adversarial learning strategies, commonly used for domain adaptation (DA), offer a robust solution in scenarios where there is substantial image variability and a lack of labeled images in source domains but an abundance of unlabeled images in target domains. By leveraging unannotated data from potentially different but related domains and broader distributions, we can considerably improve the performance of the image classifier.

In this study, we used 982 unannotated images from the library as the target dataset and 1000 annotated images with known HCV viral loads as the source dataset. We adopted a clinical cutoff of 1000 IU/ml, in accordance with the treatment guidelines for hepatitis C provided by the EASL (*21*, *55*–*57*). The network operated as a binary classifier, distinguishing between samples with HCV viral loads of ≥1000 IU/ml (positive) and <1000 IU/ml (negative). During training, both classifier loss and adversarial (transfer) loss were minimized concurrently, with a higher emphasis placed on minimizing the classifier loss. The loss curves of the best-performing model, shown in Fig. 3B, demonstrate strong classifier performance and model adaptation, as evidenced by low classifier loss and transfer loss. We trained three replicate models to evaluate model robustness. In our validation set, all three models performed with a perfect accuracy of 100% ($n = 3$ seed replicates; 127 spiked HCV samples). The algorithm was designed to operate with pixel quality commonly available in most consumer cameras. During preprocessing, the algorithm resizes and restructures images to optimally capture bubble signal information for analysis. The primary user-dependent requirement is to ensure that the bubble signal data are discernible to the naked eye, meaning the image must be in focus.

Assay validation with patient samples

We evaluated the clinical performance of the qualitative AAS using 38 non-AI/AN HCV-infected patient plasma samples and 36 AI/AN HCV-infected patient plasma samples through receiver operating characteristic (ROC) curve analysis (Fig. 4, A to C). The area under the curve (AUC) values were 0.997 for non-AI/AN samples, 0.981 for AI/AN samples, and 0.983 for the combined samples. The assay demonstrated sensitivities of 96.30% (95% CI, 81.03 to 99.91%) for non-AI/AN HCV patient samples, 92.31% (95% CI, 74.87 to 99.05%) for AI/AN HCV patient samples, and 94.34% (95% CI, 84.34 to 98.82%) for the combined samples in classifying HCV-infected samples with a clinically relevant viral load threshold of 1000 IU/ml based on EASL recommendations (tables S5 to S7). The specificities were 90.91% (95% CI, 58.72 to 99.77%) for non-AI/AN HCV patient samples, 100.00% (95% CI, 69.15 to 100.00%) for AI/AN HCV patient samples, and 95.24% (95% CI, 76.18 to 99.88%) for the combined samples (tables S5 to S7).

These findings strongly support the system's ability to accurately classify patient plasma samples based on a clinically relevant viral load threshold of 1000 IU/ml. The high AUC values highlight the AAS's substantial discriminatory capacity, making it suitable for clinical use and improving the accuracy of virus detection. The vertical scatterplots in Fig. 4 (D to I) show the correlation between

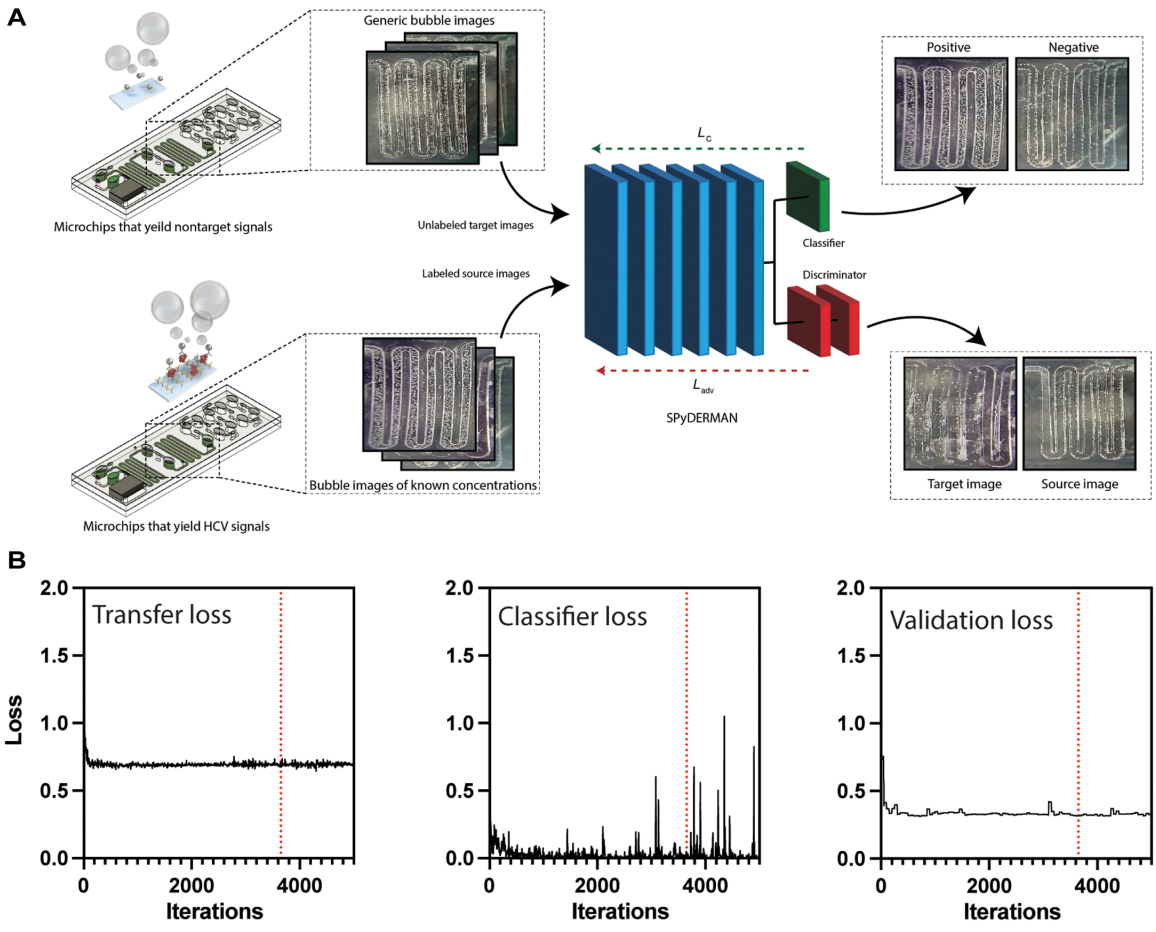

Fig. 3. Development and evaluation of the developed deep learning framework for HCV detection using spiked samples. (**A**) Schematic illustrates the general architecture and developmental pipeline of the adversarial network used in this study. L_c and L_{adv} represent classifier loss and transfer loss, with a library containing 896 unannotated images, and 420 labeled images (225 positive and 195 negative) using spiked samples. (**B**) Transfer, classifier, and validation loss curves of the network over the course of development. The dotted lines represent the iteration where the model was saved due to early stoppage conditions (lowest validation loss) in place. Validation loss was obtained at 50 iteration intervals when evaluating the validation set during training. The classifier and transfer loss represent the training losses.

qualitative AAS results and PCR outcomes for patient samples, highlighting specific discrepancies. To further assess the performance of AAS with low HCV viral loads, which is critical to early detect the newly infected individuals in high risk groups (*58*), we conducted an evaluation using 23 low viral load samples with viral loads bellow 5000 IU/ml (*59*). The assay demonstrated a robust performance, accurately detecting HCV in 22 samples, with only one false negative observed. These findings provide strong evidence supporting the reliability and validity of the calculated LODs for the assay, as presented in tables S3 and S4. This alignment, corroborated by Pearson's and Spearman's correlation coefficients, underscores the robustness of the association between these variables.

DISCUSSION

HCV infection poses a formidable global health challenge, affecting an estimated 58 million individuals worldwide, with 1.5 million new infections emerging annually. If left untreated, then HCV can progress to severe conditions such as cirrhosis and hepatocellular carcinoma. Despite recent strides in cost-effective HCV treatments, rapid and early detection of active cases remains a key hurdle, especially for those disproportionately affected by HCV infection such as AI/ANs. Alarmingly, only 21% of HCV-infected individuals receive a diagnosis globally, underscoring the urgent need for improved screening strategies.

Of particular concern are AI/AN populations, who bear a disproportionate burden of HCV infection. They experience a rate of 2.9 cases per 100,000 compared to 0.5 cases per 100,000 in African Americans and 1.2 cases per 100,000 in non-Hispanic whites, with higher mortality rates. Achieving the WHO's HCV elimination targets, aiming for an 80% reduction in new infections and a 65% reduction in HCV-related mortality by 2030, requires substantial improvements in screening efforts. The existing two-step HCV testing protocol, involving initial antibody testing followed by confirmatory RNA testing, proves costly and time-consuming, leading to attrition in HCV management. In June 2024, the FDA approved Cepheid's Xpert HCV test and the GeneXpert Xpress System, making it the first hepatitis C test available for use in certified POC settings for individuals at risk (*60*). However, the high cost of the GeneXpert system, approximately $25,000 for the analyzer, along

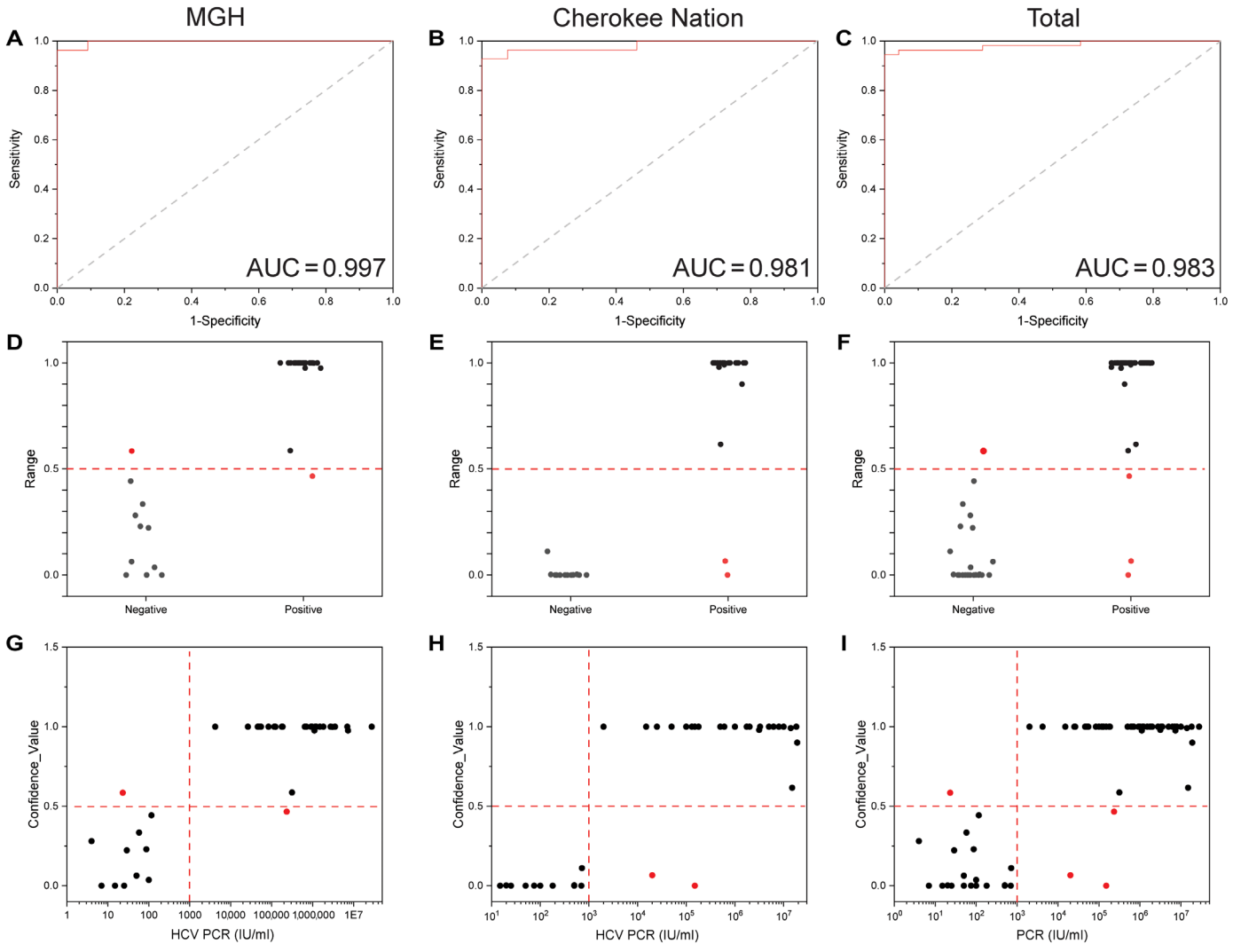

Fig. 4. Assay validation with patient samples. ROC analysis using clinical samples from patients at (**A**) MGH ($n = 38$), (**B**) Cherokee Nation Specialty Clinic ($n = 36$), and (**C**) both ($n = 74$). Vertical scatterplots for clinical samples collected from MGH (**D**), Cherokee Nation (**E**), and both sites (**F**). Qualitative AAS results depending on PCR quantitative testing results of clinical samples collected from MGH (**G**), Cherokee Nation (**H**), and both sites (**I**). Due to the limited availability of patient samples with viral concentrations near the LODs, 10 spiked clinical samples with concentrations close to the cutoff were included to better assess the assay's performance in the critical range.

with its limited portability as a benchtop device, has restricted its widespread accessibility (*61*).

An alternative approach lies in cost-effective, rapid, sensitive, and specific POC HCV Ag testing, offering potential for streamlined screening and diagnosis in a single step. However, commercially available and FDA-approved devices for POC HCV Ag testing are currently lacking. Most existing assays are laboratory-based, relatively costly, and lack the necessary sensitivity and specificity, particularly for samples with low viral loads (<1000 IU/ml).

To bridge this clinical gap, we developed and validated an affordable, rapid, sensitive, and specific POC HCV Ag diagnostic assay through seamless integration of nanotechnology, microfluidics, and deep learning–based image processing. We used the catalytic properties of PtNPs to generate bubbling signals, achieving high analytical sensitivity capable of detecting HCV at concentrations as low as 574 IU/ml. Our image-based inferences were facilitated by the adversarial-based SPyDERMAN network, which was trained on a limited dataset consisting of images of microchips with bubble signals from tests with known HCV concentrations and a large retrospective library of nonspecific bubbling-microchip images. This HCV detection device is user-friendly, cost-effective, and portable, aiming to reduce HCV-related health disparities by improving accessibility for underserved communities, particularly AI/AN populations, thereby enhancing equity in HCV-related care. Table S8 provides a comparative analysis of the AAS (HCV cAg immunoassay) alongside several other diagnostic assays for HCV detection. It highlights key performance characteristics, including sensitivity, specificity, detection targets, LOD, portability, automation capabilities, cost, time to result, and commercialization status. The AAS assay demonstrates high sensitivity (94.34%) and specificity (95.24%), with a relatively rapid time to result (23 min) and low cost, positioning it as a promising option for resource-limited settings. In contrast, other assays such as the Elecsys Anti-HCV and Architect

Anti-HCV assays exhibit perfect sensitivity and specificity but lack portability and are typically more costly. The table also includes emerging nucleic acid–based assays, some of which offer impressive LOD values but are in research stages, highlighting ongoing advancements in HCV diagnostics.

The developed platform demonstrates remarkable adaptability beyond HCV detection, showcasing notable potential for identifying a wide array of pathogens and biomarkers. The SPyDERMAN framework used in the system can be easily expanded using relatively small annotated datasets tailored to other biotargets. In addition, the microfluidic cartridge design can be modified to include multiple parallel detection channels, enabling multiplexing for the simultaneous detection of various biomarkers (*54*). This capability has been validated in prior studies, where microfluidic platforms were effectively adapted for analyzing diverse biomarkers with high accuracy and minimal cross-reactivity (*62*). By incorporating multiplexed detection and leveraging advancements in deep learning, the platform can tackle a variety of diagnostic challenges, such as coinfections and differential diagnoses of diseases with overlapping symptoms. These enhancements further establish the platform as a versatile and comprehensive tool for POC diagnostics across a wide range of applications.

Shelf life is crucial for POC devices, and we have previously investigated this by using trehalose as a natural stabilization agent for long-term storage of immuno-functionalized microfluidic devices (*63*). Alternatively, freeze-drying the surface chemistry on-chip has also demonstrated long-term (>200 days) stability (*64*). In addition, we have previously evaluated the stability of the antibody-functionalized chips and have shown its stability for 45 days when lyophilized and stored at room temperature (*65*) We also previously assessed the effects of temperature, humidity, and hydrogen peroxide concentration on the bubble signal. The stability of the developed bubble approach was maintained under different environmental conditions (*65*). We also tested the effect of H_2O_2 concentration on bubble formation and sample detection and observed that variations in H_2O_2 concentration did not notably affect the number of bubbles or the qualitative detection of samples (*65*).

The long-term reliability of our HCV detection device is attributed to the stable catalytic activity and durability of PtNPs, as demonstrated in comparable diagnostic systems (*65*). PtNPs exhibit exceptional resistance to degradation, retaining their catalytic efficiency over prolonged periods—an essential feature for consistent assay performance in resource-limited environments (*65*). Furthermore, the use of microfluidic components made from PMMA ensures both durability and compatibility with high-volume manufacturing techniques (*51*). Studies show that antibody-functionalized microchannels, reinforced with a PEI coating, maintain high binding efficiency over multiple operational cycles (*51*). By leveraging cost-effective, scalable manufacturing processes such as injection molding, the device achieves a balance of reliability and affordability. In addition, its automated design and low maintenance requirements enhance ease of use and minimize the risk of operational errors, making it well-suited for long-term deployment in POC applications.

In summary, the reported POC HCV Ag assay stands as a promising solution to enhance access to HCV care, especially for populations disproportionately affected, providing a comprehensive and accessible approach to diagnosis in resource-limited settings and populations experiencing HCV-related health disparities.

MATERIALS AND METHODS

Materials

All materials are commercially available. Details are provided in the Supplementary Materials.

Preparation of detection antibody conjugated with PtNPs

For the preparation of anti-HCV cAg antibody conjugated PtNPs (Nanoprobes), anti-HCV cAg antibody was firstly processed with buffer exchange with 4 mM sodium citrate buffer to prevent aggregations of PtNP using a Zeba column with 7000 molecular weight (MW) cutoff. Then, 2 μl of anti-HCV cAg antibody (2 mg/ml) was mixed with 1 ml of (0.1 mg/ml; 1.2×10^{10}/ml) 70-nm PtNPs in 4 mM sodium citrate buffer and continuously mixed using a rotator (20 rpm) at 4°C overnight. To block the PtNP surface, 400 μl of 10% BSA in 4 mM sodium citrate buffer was added into the slurry and mixed with PtNPs on a rotator (20 rpm) at 4°C overnight. Unconjugated antibodies were removed by centrifugation at 3000*g* for 2 min with 400 μl with 1% BSA in phosphate-buffered saline (PBS) buffer pH 7.4, six times. Last, the prepared nanoprobes were suspended and stored in 1 ml of PBS (pH 7.4), containing 1% BSA at 4°C.

Design and fabrication of the automated handheld microfluidic analyzer

The outer shell and inner frames of the standalone handheld reader were designed using Autodesk's Fusion 360 three-dimensional (3D) computer-aided design software, as shown in fig. S4. It consists of two parts: The top part includes three insertion slots for the disposable microfluidic cartridge, the tubing holder, and the solenoid valve, designed to ensure accurate and secure connections using adjustable alignment sleeves. The bottom part houses the microcontroller (SEEED XIAO), the micromotor drive (DRV8871), the Mini-pump (peristaltic, RP-Q1), 9-V batteries, and the power switch, with components securely attached using industrial double-sided foam tape. The two parts are assembled using four pairs of strong neodymium magnets, and the chamber components were printed using an Ultimaker S5 3D printer (UltiMaker).

Fabrication of the disposable microfluidic cartridge

The disposable microfluidic cartridge was prepared by assembling five layers of PMMA substrates, one layer of adhesive tape, three bacterial viral filters (BVFs), and a valve adapter made of polydimethylsiloxane (PDMS), as shown in fig. S2. The top, middle, and bottom layers of the PMMA substrates were cut into three identical 3.15-mm–thick substrates with different features using a laser cutter. The channel layers (1 and 2) were cut into two identical 0.2-mm–thick PMMA substrates with different features. The BVFs were cut into 2-mm discs using biopsy punches. The adhesive tape layers were cut by a Cricut Joy cutting machine. The valve adapters were cut from a 2-mm–thick PDMS sheet using biopsy punches with 8 and 1.5 mm in diameters, with a 2-mm BVF disc inserted into the middle hole (fig. S2). The PDMS sheet was made using a SYLGARD 184 silicone-based elastomeric kit, with a 1:10 curing ratio and 2 hours of curing at 70°C.

To assemble the disposable microfluidic cartridges, the PMMA substrates were bonded following a modified protocol developed by Trinh *et al.* (*66*). The PMMA substrates were first cleaned by sonicating in 10% isopropyl alcohol (IPA) in deionized water for 10 min and dried with compressed air. For bonding, 300 μl of 60% acetic acid diluted in deionized (DI) water was coated onto the surface of the bottom PMMA layer, which was then covered with the

next PMMA layer. The assembly was pressed continuously at 400 PSI for 1.5 min at 65°C to create a permanent bond. After pressure application, the remaining solution inside the microchannel was removed by vacuum, and the assembly was cured in a convection oven at 70°C for 2 hours. The PMMA assembly was then cooled to room temperature, and the microfluidic channels were rinsed with DI water and functionalized with antibodies (detailed procedures for antibody functionalization are provided in the "Functionalization of the microchannels with antibodies" section). Assay reagents, including the washing buffer and 30% hydrogen peroxide, were then loaded into the corresponding reservoirs, as shown in fig. S2. The top of the PMMA assembly was sealed with adhesive tape, with punched vents at the sample reservoir and the first and last outlets. Last, the BVF discs were inserted into the first and last outlets, and the valve adapter was attached to the vent on the sample reservoir using double-sided adhesive. The disposable microfluidic cartridges were packaged in resealable bags and stored at 4°C until use.

Functionalization of the microchannels with antibodies

To functionalize the PMMA microchannels with antibodies, we followed a modified protocol adapted from the methods developed by Feyssa *et al.* (*50*) and Bai *et al.* (*51*). Briefly, the microchannels were first washed three times with DI water. The channels were then filled with 1 M NaOH and incubated at 55°C for 30 min to hydrolyze the ester groups of PMMA. After washing the channels three more times with DI water, they were filled with 0.2% PEI (MW = 75,000, pH 11.5) and incubated at room temperature for 1 hour. The channels were then washed six times with DI water and filled with 5% (w/v) GA solution and incubated at room temperature. After another six washes with DI water, the channels were filled with antibody (50 μg/ml; diluted in PBS, pH 7.4) and incubated overnight at 4°C. The channels were then drained using a vacuum and filled with 3% BSA in tris buffer with 0.2% PAA and incubated overnight at 4°C to block unreacted groups and prevent nonspecific binding in subsequent assays. Last, the channels were washed three times with phosphate buffered saline with Tween 20 (PBST) and drained with a vacuum.

Programming and control of the solenoid valve and mini pump

To control the operation of the pump and solenoid, we designed a custom software as depicted in fig. S3. To load the running code into the analyzer, we connected a desktop computer to the Arduino chip via a Universal Serial Bus interface. After verification, we uploaded the code to the chip through the serial port (full code can be accessed via the Dryad dataset: https://doi.org/10.5061/dryad.9ghx3ffsm). Once powered, the Arduino chip can start automatically without the need of PC. The algorithm steps, shown in figs. S6 and S7, are as follows:

1) Configure ports and parameters: We set ports D1 and D2 of the chip as output ports to control the pump's movement and port D5 as an output port to control the solenoid valve switch. Parameters include the pump cycle operation period, pump forward time, pump backward time, solenoid valve switch time, and delay. These parameters are preset before uploading and can be adjusted based on experimental conditions.

2) Load samples: To load the virus sample into the control and test channels of the microfluidic chips, the solenoid valve is turned on to connect the chip's pores to the atmosphere and use the pump to push the samples into the control channel. Twenty oscillatory flows in the test channel mix the sample with the reagents. Oscillatory flow is achieved by alternating the pump's forward and backward movements with delays. The sample is then pushed into the control channel, and 10 oscillatory flows will help mixing the sample with the reagents in the control channel.

3) Washing: After loading the virus sample, the control and test channels of the microfluidic chip are washed. The solenoid valve is then turned off to connect the middle pore of the microfluidic chips to the atmosphere and push the washing buffer into the channels sequentially. The solenoid valve is then turned on, and five oscillatory flows are performed to thoroughly clean the channels. This cleaning process is repeated three times.

4) Introduce catalyzer solution: Last, the solenoid valve is turned off, and the catalyzer solution is pushed into the control and test channels through sequential flow by moving the pump forward. The catalyzer solution is incubated in the control and test channels of the cartridge for bubble signal generation.

Fabrication of the standalone detection module

The detection module, measuring 140 mm by 100 mm by 168 mm, is designed to fully cover both the testing and control channels, as shown in fig. S5. This design effectively blocks external light variations, creating a stable optical environment for precise bubble image capture. The detection module consists of an outer shell, a slot for the wireless mini CMOS, a slot for the 15× macro lens (focal length: 3 cm), a slot for the battery, and a groove to attach the white LED strip. The CMOS and lens are positioned at the center of the bottom of the module, exactly 3 cm below the microfluidic cartridge slot, ensuring focused image capture of the bubbles within the microfluidic channels. When the main power is turned on, the CMOS sensor automatically activates to capture photos with the desired parameters for further analysis.

Data acquisition by CMOS camera and quantification

The images captured with the CMOS camera were cropped with 1.5 × 3.5–inch size, and the cropped images were analyzed using ImageJ.

Investigation of antibody conjugations

The functionality of antibodies conjugated on the PMMA surface of the microfluidic channels was evaluated using FTIR spectra. As shown in fig. S7, the FTIR spectrum of pristine PMMA was compared with PMMA modified by (orange) PEI and (blue) protein + PEI coating. The PEI-coated PMMA exhibits characteristic primary amine absorptions at 3282, 2838, and 1590 cm^{-1} (indicative of NH stretching and bending), confirming successful PEI coating. The protein-PEI–coated PMMA shows characteristic absorptions at 1637 cm^{-1} (C═C stretching), 1524 cm^{-1} (N─O stretching), and 1389 cm^{-1} (S═O stretching), indicating successful antibody coating.

The functionality of antibodies conjugated on the surface of PtNPs was also evaluated using FTIR spectra. Surface FTIR spectra of the PtNPs were compared before (gray) and after (red) antibody functionalization. As shown in fig. S8, the antibody-conjugated PtNPs exhibit protein characteristic absorptions at 1652 cm^{-1} (N─H bending), 1547 cm^{-1} (N─O stretching), and 1397 cm^{-1} (C─O stretching), indicating successful antibody conjugation on the surface of the PtNPs.

Development of the deep learning classifier for HCV detection

Images were preprocessed before use for both training and testing with an adversarial network similar to our previous work to develop a data library that can be used to increase the accuracy of the classifier network without collecting thousands of real-life annotated images that are time consuming (*54*). Briefly, the microfluidic channels of the chips imaged with the camera were isolated by cropping the images and the channels were resized (256 pixels by 256 pixels).

In this study, a deep learning model was developed for HCV detection and integrated with a fully automated microfluidic channels using the SPyDERMAN platform (*54*). Previously, this platform was used for detection of other viruses such as HIV and in the detection of fentanyl (CITATIONS). The network leverages unannotated data from a data library by framing the problem as a DA challenge (*54*, *67*). SPyDERMAN's adversarial network, which incorporates MD-nets, minimizes domain discrepancies between feature representations of source and target images while reducing classifier error. The network is composed of three main components: a feature extractor, a classification layer, and an adversarial block.

The Xception architecture was used as the feature extractor. The combined losses from the classifier block and adversarial block were minimized using the total loss function

$$L_{\text{total}}: \min[\varepsilon(C) - \lambda\varepsilon(D)]$$

where $\varepsilon(C)$ represents the classifier loss L_c and $\varepsilon(D)$ represents the adversarial (transfer) loss L_{adv}. The classifier loss, $\varepsilon(C)$, is defined as

$$E_{(X_i^s, Y_i^s)\sim D_s} L[C(X_i^s), Y_i^s]$$

with X_i^s and Y_i^s representing the source images and their respective ground truth annotations. The loss $L()$ is a cross-entropy loss, and $C()$is the classifier network. The adversarial loss, $\varepsilon(D)$, is given by

$$-E_{x_i^s\sim D_s} w[H(c_i^s)]\log\left[D(h_i^s)\right] - E_{x_j^t\sim D_t} w\left[H\left(c_j^t\right)\right]\log\left[1 - D\left(h_j^t\right)\right]$$

where $w[H(c)]$ represents the weighted uncertainty of predictions and h is a multilinear feature map that combines class confidence and feature representations. The trade-off parameter λ was set to 0.5 in this study and optimized during training to balance classifier and adaptation performance.

Training data were loaded in batches of 16, with data augmentations such as rotations and flips applied with a probability of 0.5. The optimization was performed using Adam with an initial learning rate of 0.0001 and a weight decay of 0.0005. An L2 penalty was applied to prevent overfitting. The learning rate was adjusted according to the formula

$$lr = lr_0 \times (1 + \gamma \times i)^{-\text{power}}$$

where γ was set to 0.0001, the power to 0.75, and i denoted the training progress. A momentum of 0.9 was used to accelerate learning. The optimal batch size and learning rate were manually determined on the basis of the lowest validation loss. The images were resized to 256 pixels, with a crop size of 224 pixels. The training process consisted of five iterations, with early stoppage patience set to 2000 iterations. Validation was performed every 50 iterations, and model snapshots were taken every 1000 iterations to monitor performance. The network capitalizes on adversarial training, leveraging unlabeled nonspecific bubble signal data.

A library containing 896 unannotated images was developed specifically for the automated microfluidic channels. The network transforms both annotated HCV data (source) and nonannotated data from the library (target) into feature representations via the feature extractor. These representations are used by the classifier and adversarial blocks during training to accurately classify HCV samples as positive or negative. SPyDERMAN focuses on retaining class-specific features despite domain shifts from source to target. The data library enhances the distribution of data by incorporating variabilities such as bubble shapes, sizes, concentrations, and positions, thereby improving the network's generalizability. The code can be accessed via https://github.com/shafieelab/SPyDERMAN.

Biosafety and human participant statement

The research work reported was approved and performed in adherence to guidelines and procedures approved by the Institutional Biosafety Committee of Mass General Brigham (parent organization of Massachusetts General Hospital (MGH) and Brigham and Women's Hospital) and under appropriate institutional review boards (IRBs) (MGB IRB nos. 2023P000538 and 2014P002784). This study was approved by the Cherokee Nation IRB. Patient enrollment was voluntary, and informed consent was required for participation. Except for the member of Cherokee Nation Health Services, we do not have access to identifiable information. All the experiments with HCV patient samples were performed in a Biosafety Level 2+ (BSL2+) laboratory. Non-AI/AN HCV patient plasma samples were received from MGH and AI/AN HCV patient plasma samples were received from the Cherokee Nation Health Service through J. Mera. The viral loads of the samples were measured using a standard RT-PCR system at MGH, Cherokee Nations through a third party referral laboratory vendor, or a third party vendor (Eurofins Viracor). The spiked samples that were used in system testing throughout the study were prepared by serial dilutions of stock virus samples with known viral loads measured by standard PCR approaches. In these cases, the control samples were virus-free samples that were processed for the detection assay with the same protocol as the viral samples, except for the addition of viral-stock dilutions.

Statistical analysis

Statistical analyses were performed using Origin software version 8.5 (OriginLab Corporation, Northampton, MA, USA). All viral load values were converted into $\log_{10}$ IU/ml. The mean and SDs were calculated for each data point from at least a total of two to three independent experiments unless indicated in the text. The level of significance was set at $P > 0.05$. ROC and scattering plots analysis were used to define performance of AAS to the standard analytical technique. The strength of the linear and nonlinear relationship was evaluated using Pearson's correlation and Spearman correlation, respectively.

Large language models

The authors exclusively authored the entire manuscript. ChatGPT 4o was solely used for addressing typographical errors and making text edits. The following prompt was used: "Please revise the draft, checking the typos and grammar errors."

Reporting summary

Further information on research design is available in the Nature Research Reporting Summary linked to this article.

Supplementary Materials

The PDF file includes:

Supplementary Text

Figs. S1 to S12
Tables S1 to S8
Legends for movies S1 to S3
References

Other Supplementary Material for this manuscript includes the following:
Movies S1 to S3

REFERENCES AND NOTES

1. World Health Organization (WHO), *Global progress report on HIV, viral hepatitis and sexually transmitted infections, Accountability for the global health sector strategies 2016–2021: Actions for impact* (WHO, 2021); www.who.int/publications/i/item/9789240027077.
2. J. Mera, C. Vellozzi, S. Hariri, H. Carabin, D. A. Drevets, A. Miller, B. Reilley, W. Essex, D. Gahn, L. Lyons, J. Leston, J. W. Ward, Identification and clinical management of persons with Chronic Hepatitis C virus infection - Cherokee nation, 2012-2015. *MMWR Morb. Mortal. Wkly. Rep.* **65**, 461–466 (2016).
3. CDC, Hepatitis tables and figures - US 2017 surveillance data for viral hepatitis (CDC, 2019); https://archive.cdc.gov/www_cdc_gov/hepatitis/statistics/2017surveillance/index.htm.
4. N. A. John-Henderson, E. J. White, T. L. Crowder, Resilience and health in American Indians and Alaska Natives: A scoping review of the literature. *Dev. Psychopathol.* **35**, 2241–2252 (2023).
5. J. A. Gutierrez, E. J. Lawitz, F. Poordad, Interferon-free, direct-acting antiviral therapy for chronic hepatitis C. *J. Viral Hepat.* **22**, 861–870 (2015).
6. AASLD/IDSA HCV Guidance Panel, Hepatitis C guidance: AASLD-IDSA recommendations for testing, managing, and treating adults infected with hepatitis C virus. *Hepatology* **62**, 932–954 (2015).
7. C. M. Denkinger, M. Kessel, Diagnostics for hepatitis C: An urgent need for action. *Lancet Glob. Health.* **3**, e195 (2015).
8. WHO, "Global Hepatitis Report" (WHO, 2017); http://apps.who.int/iris/bitstream/10665/255016/1/9789241565455-eng. pdf?ua=1.
9. Global Burden of Disease Study 2013 Collaborators, Global, regional, and national incidence, prevalence, and years lived with disability for 301 acute and chronic diseases and injuries in 188 countries, 1990-2013: A systematic analysis for the Global Burden of Disease Study 2013. *Lancet* **386**, 743–800 (2015).
10. E. Ivanova Reipold, P. Easterbrook, A. Trianni, N. Panneer, D. Krakower, S. Ongarello, T. Roberts, V. Miller, C. Denkinger, Optimising diagnosis of viraemic hepatitis C infection: The development of a target product profile. *BMC Infect. Dis.* **17**, 707 (2017).
11. WHO, Global health strategy on viral hepatitis 2016–2021 (WHO, 2016); https://apps.who.int/iris/bitstream/handle/10665/246177/WHO-HIV-2016.06-eng.pdf.
12. D. Tordrup, Y. Hutin, K. Stenberg, J. A. Lauer, D. W. Hutton, M. Toy, N. Scott, M. Bulterys, A. Ball, G. Hirnschall, Additional resource needs for viral hepatitis elimination through universal health coverage: Projections in 67 low-income and middle-income countries, 2016-30. *Lancet Glob. Health* **7**, e1180–e1188 (2019).
13. M. G. Ghany, D. B. Strader, D. L. Thomas, L. B. Seeff, American Association for the Study of Liver Diseases, Diagnosis, management, and treatment of hepatitis C: An update. *Hepatology* **49**, 1335–1374 (2009).
14. CDC, Testing for HCV infection: An update of guidance for clinicians and laboratorians (CDC, 2013); www.cdc.gov/mmwr/preview/mmwrhtml/mm6218a5.htm.
15. J. J. Feld, J. W. Ward, Key elements on the pathway to HCV elimination: Lessons learned from the AASLD HCV special interest group 2020. *Hepatol. Commun.* **5**, 911–922 (2021).
16. D. L. Thomas, Global elimination of chronic hepatitis. *N. Engl. J. Med.* **380**, 2041–2050 (2019).
17. J. M. Pawlotsky, Diagnostic tests for hepatitis C. *J. Hepatol.* **31**, 71–79 (1999).
18. N. Hanuka, E. Sikuler, D. Tovbin, M. Mostoslavsky, M. Hausman, M. Orgel, A. Yaari, Y. Shemer-Avni, Hepatitis C virus infection in renal failure patients in the absence of anti-hepatitis C virus antibodies. *J. Viral Hepat.* **9**, 141–145 (2002).
19. CDC, Testing recommendations for hepatitis C virus infection (CDC, 2016); https://www.cdc.gov/hepatitis-c/hcp/diagnosis-testing/?CDC_AAref_Val=https://www.cdc.gov/hepatitis/hcv/guidelinesc.htm.
20. K. G. Pollock, S. A. McDonald, R. Gunson, A. M. Leod, A. Went, D. J. Goldberg, S. J. Hutchinson, S. T. Barclay, Real-world utility of HCV core antigen as an alternative to HCV RNA testing: Implications for viral load and genotype. *J. Viral Hepat.* **27**, 996–1002 (2020).
21. J. M. Pawlotsky, F. Negro, A. Aghemo, M. Berenguer, O. Dalgard, G. Dusheiko, F. Marra, M. Puoti, H. Wedemeyer, European Association for the Study of the Liver. Electronic address: easloffice@easloffice.eu, Clinical Practice Guidelines Panel: Chair, EASL Governing Board representative, Panel members, EASL recommendations on treatment of hepatitis C: Final update of the series. *J. Hepatol.* **73**, 1170–1218 (2020).
22. C. P. Jülicher, V. P. Chulanov, N. N. Pimenov, E. Chirkova, C. A. Yankina, Streamlining the screening cascade for active Hepatitis C in Russia: A cost-effectiveness analysis. *PLOS ONE* **14**, e0219687 (2019).
23. M. van Tilborg, S. H. Al Marzooqi, W. W. L. Wong, R. Maan, J. Vermehren, B. Maasoumy, T. Mazzulli, S. Bolotin, G. Garber, F. Guerra, C. R. Flud, M. Kowgier, H. L. Janssen, R. J. de Knegt, J.-M. Pawlotsky, G. A. Cloherty, A. Duarte-Rojo, C. Sarrazin, H. Wedemeyer, J. J. Feld, HCV core antigen as an alternative to HCV RNA testing in the era of direct-acting antivirals: Retrospective screening and diagnostic cohort studies. *Lancet Gastroenterol. Hepatol.* **3**, 856–864 (2018).
24. F. Fabrizi, G. Lunghi, F. Aucella, S. Mangano, F. Barbisoni, S. Bisegna, D. Vigilante, A. Limido, P. Martin, Novel assay using total hepatitis C virus (HCV) core antigen quantification for diagnosis of HCV infection in dialysis patients. *J. Clin. Microbiol.* **43**, 414–420 (2005).
25. K. Aoyagi, C. Ohue, K. Iida, T. Kimura, E. Tanaka, K. Kiyosawa, S. Yagi, Development of a simple and highly sensitive enzyme immunoassay for hepatitis C virus core antigen. *J. Clin. Microbiol.* **37**, 1802–1808 (1999).
26. T. Kaiser, H. C. Damerow, S. Tenckhoff, A. Finger, I. Böttcher, C. Hafer, A. Schwarz, J. B. Lüth, H. S. Gürtler, G. Colucci, M. P. Manns, H. Wedemeyer, H. L. Tillmann, Kinetics of hepatitis C viral RNA and HCV-antigen during dialysis sessions: evidence for differential viral load reduction on dialysis. *J. Med. Virol.* **80**, 1195–1201 (2008).
27. C. G. Schüttler, C. Thomas, T. Discher, G. Friese, J. Lohmeyer, R. Schuster, S. Schaefer, W. H. Gerlich, Variable ratio of hepatitis C virus RNA to viral core antigen in patient sera. *J. Clin. Microbiol.* **42**, 1977–1981 (2004).
28. K. Seme, M. Poljak, D. Z. Babic, T. Mocilnik, A. Vince, The role of core antigen detection in management of hepatitis C: A critical review. *J. Clin. Virol.* **32**, 92–101 (2005).
29. M. Bouvier-Alias, K. Patel, H. Dahari, S. Beaucourt, P. Larderie, L. Blatt, C. Hezode, G. Picchio, D. Dhumeaux, A. U. Neumann, J. G. McHutchison, J.-M. Pawlotsky, Clinical utility of total HCV core antigen quantification: A new indirect marker of HCV replication. *Hepatology* **36**, 211–218 (2002).
30. M. Lemoine, K. Lacombe, HCV core antigen: Toward elimination of nucleic acid testing? *Lancet Gastroenterol. Hepatol.* **3**, 817–818 (2018).
31. S. Laperche, C. M. Nübling, S. L. Stramer, E. Brojer, P. Grabarczyk, H. Yoshizawa, V. Kalibatas, M. E. Elkyabi, F. Moftah, A. Girault, H. van Drimmelen, M. P. Busch, N. Lelie, Sensitivity of hepatitis C virus core antigen and antibody combination assays in a global panel of window period samples. *Transfusion* **55**, 2489–2498 (2015).
32. A. Rokuhara, E. Tanaka, A. Matsumoto, T. Kimura, T. Yamaura, K. Orii, X. Sun, S. Yagi, N. Maki, K. Kiyosawa, Clinical evaluation of a new enzyme immunoassay for hepatitis B virus core-related antigen; a marker distinct from viral DNA for monitoring lamivudine treatment. *J. Viral Hepat.* **10**, 324–330 (2003).
33. E. Tanaka, C. Ohue, K. Aoyagi, K. Yamaguchi, S. Yagi, K. Kiyosawa, H. J. Alter, Evaluation of a new enzyme immunoassay for hepatitis C virus (HCV) core antigen with clinical sensitivity approximating that of genomic amplification of HCV RNA. *Hepatology* **32**, 388–393 (2000).
34. J. Lorenzo, A. Castro, A. Aguilera, E. Prieto, S. López-Calvo, B. Regueiro, J. Pedreira, Total HCV core antigen assay. A new marker of HCV viremia and its application during treatment of chronic hepatitis C. *J. Virol. Methods* **120**, 173–177 (2004).
35. A. R. Zanetti, L. Romanò, M. Brunetto, M. Colombo, G. Bellati, C. Tackney, Total HCV core antigen assay: A new marker of hepatitis C viremia for monitoring the progress of therapy. *J. Med. Virol.* **70**, 27–30 (2003).
36. P. Veillon, C. Payan, G. Picchio, M. Maniez-Montreuil, P. Guntz, F. Lunel, Comparative evaluation of the total hepatitis C virus core antigen, branched-DNA, and amplicor monitor assays in determining viremia for patients with chronic hepatitis C during interferon plus ribavirin combination therapy. *J. Clin. Microbiol.* **41**, 3212–3220 (2003).
37. K. Morota, R. Fujinami, H. Kinukawa, T. Machida, K. Ohno, H. Saegusa, K. Takeda, A new sensitive and automated chemiluminescent microparticle immunoassay for quantitative determination of hepatitis C virus core antigen. *J. Virol. Methods* **157**, 8–14 (2009).
38. M. C. Medici, G. Furlini, A. Rodella, A. Fuertes, A. Monachetti, A. Calderaro, S. Galli, L. Terlenghi, M. Olivares, P. Bagnarelli, A. Costantini, F. De Conto, M. Sainz, C. Galli, N. Manca, M. P. Landini, G. Dettori, C. Chezzi, Hepatitis C virus core antigen: Analytical performances, correlation with viremia and potential applications of a quantitative, automated immunoassay. *J. Clin. Virol.* **51**, 264–269 (2011).
39. A. R. Garbuglia, A. Monachetti, C. Galli, R. Sabatini, M. L. Ferreri, M. R. Capobianchi, P. Bagnarelli, HCV core antigen and HCV-RNA in HIV/HCV co-infected patients with different HCV genotypes. *BMC Infect. Dis.* **14**, 222 (2014).
40. C. Ottiger, N. Gygli, A. R. Huber, Detection limit of architect hepatitis C core antigen assay in correlation with HCV RNA, and renewed confirmation algorithm for reactive anti-HCV samples. *J. Clin. Virol.* **58**, 535–540 (2013).
41. J. M. Freiman, T. M. Tran, S. G. Schumacher, L. F. White, S. Ongarello, J. Cohn, P. J. Easterbrook, B. P. Linas, C. M. Denkinger, Hepatitis C core antigen testing for diagnosis of hepatitis C virus infection: A systematic review and meta-analysis. *Ann. Intern. Med.* **165**, 345–355 (2016).
42. B. Bertisch, M. Brezzi, F. Negro, B. Müllhaupt, C. Ottiger, P. Künzler-Heule, P. Schmid, F. Giudici, O. Clerc, A. Moriggia, M. Roelens, F. Marinucci, C. Zehnder, D. Moradpour, O. Keiser, Swiss Hepatitis C Cohort Study, Very low hepatitis C viral loads in treatment-naive persons: Do they compromise hepatitis C virus antigen testing? *Clin. Infect. Dis.* **70**, 653–659 (2020).

43. WHO, "WHO public reports for in-vitro diagnostics" (WHO, 2021); https://extranet.who.int/prequal/vitro-diagnostics/prequalification-reports/whopr.
44. S. D. Warkad, K. S. Song, D. Pal, S. B. Nimse, Developments in the HCV screening technologies based on the detection of antigens and antibodies. *Sensors (Basel)* **19**, 4257 (2019).
45. C. Wang, L. Zhang, X. Shen, Development of a nucleic acid lateral flow strip for detection of hepatitis C virus (HCV) core antigen. *Nucleosides Nucleotides Nucleic Acids* **32**, 59–68 (2013).
46. J. A. Frimpong, T. D'Aunno, D. C. Perlman, S. M. Strauss, A. Mallow, D. Hernandez, B. R. Schackman, D. J. Feaster, L. R. Metsch, On-site bundled rapid HIV/HCV testing in substance use disorder treatment programs: Study protocol for a hybrid design randomized controlled trial. *Trials* **17**, 117 (2016).
47. C. P. Price, Point-of-care testing. Impact on medical outcomes. *Clin. Lab. Med.* **21**, 285–303 (2001).
48. APHL, Identifying High-Priority Diagnostic Approaches for Advancing Hepatitis C Elimination in the US (APHL, 2021); https://www.aphl.org/aboutAPHL/publications/Documents/ID-HCV-2021-Meeting-Report.pdf.
49. S. Lee, W. Lee, H. Kim, P. K. Bae, J. Park, J. Kim, Oscillatory flow-assisted efficient target enrichment with small volumes of sample by using a particle-based microarray device. *Biosens. Bioelectron.* **131**, 280–286 (2019).
50. Y. Bai, C. G. Koh, M. Boreman, Y.-J. Juang, I.-C. Tang, L. J. Lee, S.-T. Yang, Surface modification for enhancing antibody binding on polymer-based microfluidic device for enzyme-linked immunosorbent assay. *Langmuir* **22**, 9458–9467 (2006).
51. B. Feyssa, C. Liedert, L. Kivimaki, L.-S. Johansson, H. Jantunen, L. Hakalahti, Patterned immobilization of antibodies within roll-to-roll hot embossed polymeric microfluidic channels. *PLOS ONE* **8**, e68918 (2013).
52. A. Shrivastava, V. B. Gupta, Methods for the determination of limit of detection and limit of quantitation of the analytical methods. *Chron. Young Sci.* **2**, 21–25 (2011).
53. D. A. Armbruster, T. Pry, Limit of blank, limit of detection and limit of quantitation. *Clin. Biochem. Rev.* **29**, S49–S52 (2008).
54. A. Shokr, L. G. C. Pacheco, P. Thirumalaraju, M. K. Kanakasabapathy, J. Gandhi, D. Kartik, F. S. R. Silva, E. Erdogmus, H. Kandula, S. Luo, X. G. Yu, R. T. Chung, J. Z. Li, D. R. Kuritzkes, H. Shafiee, Mobile health (mHealth) viral diagnostics enabled with adaptive adversarial learning. *ACS Nano* **15**, 665–673 (2021).
55. J. M. Freiman, J. Wang, P. J. Easterbrook, C. R. Horsburgh, F. Marinucci, L. F. White, G. Kamkamidze, M. Krajden, A. Loarec, R. Njouom, K. V. Nguyen, G. Shiha, R. Soliman, S. S. Solomon, T. Tsertsvadze, C. M. Denkinger, B. Linas, Deriving the optimal limit of detection for an HCV point-of-care test for viraemic infection: Analysis of a global dataset. *J. Hepatol.* **71**, 62–70 (2019).
56. D. P. Webster, P. Klenerman, G. M. Dusheiko, Hepatitis C. *Lancet* **385**, 1124–1135 (2015).
57. H. S. Yee, M. F. Chang, C. Pocha, J. Lim, D. Ross, T. R. Morgan, A. Monto, Department of Veterans Affairs Hepatitis C Resource Center Program, National Hepatitis C Program Office, Update on the management and treatment of hepatitis C virus infection: Recommendations from the Department of Veterans Affairs Hepatitis C Resource Center Program and the National Hepatitis C Program Office. *Am. J. Gastroenterol.* **107**, 669–689 (2012).
58. H.-Y. Sun, W.-D. Liu, C.-W. Wang, Y.-J. Wei, K.-Y. Lin, Y.-S. Huang, L.-H. Su, Y.-T. Chen, W.-C. Liu, Y.-C. Su, Y.-W. Chen, Y.-C. Chuang, P.-L. Lu, C.-C. Hung, M.-L. Yu, Performance of hepatitis C virus (HCV) core antigen assay in the diagnosis of recently acquired HCV infection among high-risk populations. *Microbiol. Spectr.* **10**, e0034522 (2022).
59. T. Yang, L. G. Kessler, M. J. Thompson, B. R. Lutz, Requirements and study designs for U.S. regulatory approval of influenza home tests. *J. Clin. Microbiol.* **60**, e0188421 (2022).
60. US Food and Drug Administration, FDA Permits Marketing of First Point-of-Care Hepatitis C RNA Test (2024); https://www.fda.gov/news-events/press-announcements/fda-permits-marketing-first-point-care-hepatitis-c-rna-test.
61. M. Iwamoto, A. Calzia, A. Dublineau, F. Rouet, J. Nouhin, S. Yann, S. Pin, C. Sun, K. Sann, C. Dimanche, C. Lastrucci, R. M. Coulborn, D. Maman, J.-P. Dousset, A. Loarec, Field evaluation of GeneXpert® (Cepheid) HCV performance for RNA quantification in a genotype 1 and 6 predominant patient population in Cambodia. *J Viral Hepat* **26**, 38–47 (2019).
62. F. Chen, Q. Hu, H. Li, Y. Xie, L. Xiu, Y. Zhang, X. Guo, K. Yin, Multiplex detection of infectious diseases on microfluidic platforms. *Biosensors (Basel)* **13**, 410 (2023).
63. W. Asghar, M. Yuksekkaya, H. Shafiee, M. Zhang, M. O. Ozen, F. Inci, M. Kocakulak, U. Demirci, Engineering long shelf life multi-layer biologically active surfaces on microfluidic devices for point of care applications. *Sci. Rep.* **6**, 21163 (2016).
64. C. D. Chin, T. Laksanasopin, Y. K. Cheung, D. Steinmiller, V. Linder, H. Parsa, J. Wang, H. Moore, R. Rouse, G. Umviligihozo, E. Karita, L. Mwambarangwe, S. L. Braunstein, J. van de Wijgert, R. Sahabo, J. E. Justman, W. El-Sadr, S. K. Sia, Microfluidics-based diagnostics of infectious diseases in the developing world. *Nat. Med.* **17**, 1015–1019 (2011).
65. M. S. Draz, A. Vasan, A. Muthupandian, M. K. Kanakasabapathy, P. Thirumalaraju, A. Sreeram, S. Krishnakumar, V. Yogesh, W. Lin, X. G. Yu, R. T. Chung, H. Shafiee, Virus detection using nanoparticles and deep neural network-enabled smartphone system. *Sci. Adv.* **6**, eabd5354 (2020).
66. K. T. L. Trinh, Q. N. Pham, N. Y. Lee, Clog-free and reliable solvent bonding of poly(methyl methacrylate) microdevice mediated by eco-friendly acetic acid at room temperature and its application for polymerase chain reaction and human cell culture. *Sens. Actuators B Chem.* **282**, 1008–1017 (2019).
67. M. K. Kanakasabapathy, P. Thirumalaraju, H. Kandula, F. Doshi, A. D. Sivakumar, D. Kartik, R. Gupta, R. Pooniwala, J. A. Branda, A. M. Tsibris, D. R. Kuritzkes, J. C. Petrozza, C. L. Bormann, H. Shafiee, Adaptive adversarial neural networks for the analysis of lossy and domain-shifted datasets of medical images. *Nat. Biomed. Eng.* **5**, 571–585 (2021).
68. S. Kim, J.-H. Kim, S. Yoon, Y.-H. Park, H.-S. Kim, Clinical performance evaluation of four automated chemiluminescence immunoassays for hepatitis C virus antibody detection. *J. Clin. Microbiol.* **46**, 3919–3923 (2008).
69. R. Zhang, L. Cai, Z. Ali, J. Wang, E. Fan, M. Wang, M. Wu, Z. Li, W. Liang, A chemiluminescence based approach to nucleic acid testing to detect HBV, HCV, and HIV-1 in blood screening. *Blood Genom.* **7**, 34–42 (2023).
70. P. Teengam, N. Nisab, N. Chuaypen, P. Tangkijvanich, T. Vilaivan, O. Chailapakul, Fluorescent paper-based DNA sensor using pyrrolidinyl peptide nucleic acids for hepatitis C virus detection. *Biosens. Bioelectron.* **189**, 113381 (2021).
71. L. T. Nguyen, S. R. Rananaware, L. G. Yang, N. C. Macaluso, J. E. Ocana-Ortiz, K. S. Meister, B. L. M. Pizzano, L. S. W. Sandoval, R. C. Hautamaki, Z. R. Fang, S. M. Joseph, G. M. Shoemaker, D. R. Carman, L. Chang, N. R. Rakestraw, J. F. Zachary, S. Guerra, A. Perez, P. K. Jain, Engineering highly thermostable Cas12b via de novo structural analyses for one-pot detection of nucleic acids. *Cell Rep. Med.* **4**, 101037 (2023).
72. R. Peng, W. Qi, T. Deng, Y. Si, J. Li, Development of surface-enhanced Raman scattering-sensing Method by combining novel Ag@Au core/shell nanoparticle-based SERS probe with hybridization chain reaction for high-sensitive detection of hepatitis C virus nucleic acid. *Anal. Bioanal. Chem.* **416**, 2515–2525 (2024).
73. K. Chittuam, S. Jampasa, T. Vilaivan, P. Tangkijvanich, N. Chuaypen, A. Avihingsanon, M. Sain, Y. Panraksa, O. Chailapakul, Electrochemical capillary-driven microfluidic DNA sensor for HIV-1 and HCV coinfection analysis. *Anal. Chim. Acta* **1265**, 341257 (2023).
74. S. M. El-Sheikh, D. I. Osman, O. I. Ali, W. G. Shousha, M. A. Shoeib, S. M. Shawky, S. M. Sheta, A novel Ag/Zn bimetallic MOF as a superior sensitive biosensing platform for HCV-RNA electrochemical detection. *Appl. Surf. Sci.* **562**, 150202 (2021).
75. T. u. H. Zia, A. u. H. Ali Shah, B. Ara, K. Gul, Label-free immunosensor for detection of hepatitis C (HCV) core antigen using ternary polypyrrole-Ag doped ZnO-exfoliated graphene nanocomposite. *Colloids Surf. A Physicochem. Eng. Asp.* **681**, 132709 (2024).
76. P. Pusomjit, P. Teengam, N. Chuaypen, P. Tangkijvanich, N. Thepsuparungsikul, O. Chailapakul, Electrochemical immunoassay for detection of hepatitis C virus core antigen using electrode modified with Pt-decorated single-walled carbon nanotubes. *Microchim. Acta.* **189**, 339 (2022).
77. S. Boonkaew, A. Yakoh, N. Chuaypen, P. Tangkijvanich, S. Rengpipat, W. Siangproh, O. Chailapakul, An automated fast-flow/delayed paper-based platform for the simultaneous electrochemical detection of hepatitis B virus and hepatitis C virus core antigen. *Biosens. Bioelectron.* **193**, 113543 (2021).

Acknowledgments

Funding: The work reported here was partially supported by the National Institute of Health under award numbers R01AI187513, R01EB033866, R01AI138800, R01AI138800-05S1, R33AI140489, R61AI140489, U54HL119145, and R01HD115677. **Author contributions:** H.C., R.T.C., G.P.F., S.R., G.L., H.S., J.G., Q.N.M., A.P., J.M.H., M.A., and Y.G. contributed to conceptualization. H.C., Yi.S., G.L., H.S., H.K., M.A., and Y.G. contributed to data curation. H.C., G.L., H.S., Q.N.M., M.A., Yi.S., S.U., and Y.G. contributed to formal analysis. R.T.C., S.R., H.S., J.M., and Y.G. contributed to funding acquisition. H.C., Yi.S., G.P.F., S.R., G.L., H.S., K.C., J.G., Q.N.M., A.P., M.A., S.K., S.U., Y.G., J.G., and G.C. contributed to investigation. H.C., Yi.S., G.P.F., S.R., G.L., H.S., K.C., H.K., Q.N.M., J.M.H., M.A., A.B., S.K., and Y.G. contributed to methodology. H.C., G.L., H.S., J.G., J.M., Y.G., and J.G. contributed to project administration. H.C., R.T.C., G.P.F., S.R., G.L., H.S., J.G., Q.N.M., J.M., Y.G., and J.G. contributed to resources. H.C., H.S., H.K., Q.N.M., J.M.H., M.A., P.T., S.U., Y.G., and M.K.K. contributed to software. H.C., H.S., J.M., and Y.G. contributed to supervision. H.C., G.L., H.S., Q.N.M., M.A., A.B., Yo.S., S.K., Y.G., and J.G. contributed to validation. H.C., S.R., Q.N.M., M.A., P.T., A.B., Yo.S., Y.G., and M.K.K. contributed to visualization. H.C., Yi.S., G.L., H.S., Q.N.M., M.A., Y.G., and M.K.K. contributed to writing—original draft. H.C., R.T.C., Yi.S., G.P.F., S.R., G.L., H.S., J.G., Q.N.M., A.P., J.M.H., M.A., P.T., A.B., J.M., Yo.S., S.K., S.U., Y.G., J.G., and G.C. contributed to writing—review and editing: all authors. **Competing interests:** J.M. has declared the following competing interests: Gilead Sciences: principal investigator in a clinical trial for COVID-19; AbbVie Pharmaceuticals: speaker Bureau and principal investigator in acute HCV treatment; Abbott Diagnostics: principal investigator in a study regarding etiologic diagnosis of community-acquired pneumonia; Roche Diagnostics: participated in one advisory board activity regarding HCV diagnostics. H. S. is an inventor and holds intellectual property rights for the reported deep learning-enabled gas bubble sensing technology, filed through Brigham and Women's Hospital and Mass General Brigham. The other authors declare that they have no competing interests. **Data and materials availability:** All data needed to evaluate the conclusions in the paper are present in the paper and/or the Supplementary

Materials. All designs for the 3D printed objects and laser cut objects used in the manuscript, running codes for the microfluidic device, and the SPyDERMAN model used for deep learning network training can all be found at the Dryad dataset https://doi.org/10.5061/dryad.9ghx3ffsm.

Submitted 24 September 2024
Accepted 12 February 2025
Published 19 March 2025
10.1126/sciadv.adt3803